

Article

Multi-Point, Multi-Objective Optimisation of Centrifugal Fans by 3D Inverse Design Method

Jiangnan Zhang ^{1,*} and Mehrdad Zangeneh ²

¹ Advanced Design Technology Ltd., London SW1P 4DU, UK

² Department of Mechanical Engineering, University College London, London WC1E 6BT, UK

* Correspondence: j.zhang@adtechnology.com or jiangnan.zhang@outlook.com

Abstract: In this paper, we present the design and optimization of a centrifugal fan with requirements of maximizing the total-to-static pressure rise and total-to-static efficiency at two operating points and the maximum torque provided by the motor power using a 3D inverse design method, a DOE (design of experiment) study, an RSM (response surface model) and a MOGA (multi-objective genetic algorithm). The fan geometry is parametrized using 13 design parameters, and 120 different designs are generated. The fan performances of all the designs at two operating conditions are evaluated through steady-state CFD simulations. The resulting design matrix is used to create an RSM based on the Kriging method and MOGA is used to search the design space using the RSM and find the optimal design.

Keywords: multi-point; multi-objective; optimization; centrifugal fans; inverse design method; DOE; RSM; MOGA

1. Introduction

Centrifugal fans are used in many applications where a relatively high-pressure rise is required in the compact size. The application can vary from household appliances [1] to industrial to air-conditioning and data center cooling applications [2–6]. Hariharan and Govarhan studied the effect of inlet clearance on the aerodynamic performance of a centrifugal blower [7]. Singh et al. performed a parametric study of the effect of blade number, TE blade angle and diameter ratio on the centrifugal fan performance based on experiments and numerical simulations [8]. Jeon investigated the effects of design parameters on the performance and noise of a centrifugal fan [9]. All the works mentioned above have been focused on the fan performance at only one point, which is the design point or BEP (best efficiency point), while for some applications the fans are required to meet multi-point requirements in terms of pressure rise, flow rate and efficiency. To tackle this kind of multi-point design and optimization problem, DOE and RSM approaches have been widely used for pumps, turbines and compressors [10–12]. Behzadmehr et al. carried out a parametric study of a backward-curved centrifugal fan using DOE using five design parameters, and each design parameter had two levels of variation [13]. The main drawback of this method is that a very small number of design parameters were used, which means other more important parameters may have been missed. Qiu et al. performed a multi-point design optimization of a high bypass ratio axial fan blade using DOE and Kriging approximation [14]. The optimized design shows 0.1% efficiency improvement at the design point but has a worse efficiency characteristic within the operation range. As it can be seen that in the literature there is not much study on the aerodynamic multi-point optimization of centrifugal fan blade shapes, this is the main reason that the authors would like to publish this work.

In this paper, we started with the design of a baseline design which meets the pressure rise requirements at two operating points using the 3D inverse design method. The fan



Citation: Zhang, J.; Zangeneh, M. Multi-Point, Multi-Objective Optimisation of Centrifugal Fans by 3D Inverse Design Method. *Int. J. Turbomach. Propuls. Power* **2023**, *8*, 8. <https://doi.org/10.3390/ijtp8010008>

Academic Editor: Thomas Carolus

Received: 27 September 2022

Revised: 3 February 2023

Accepted: 12 February 2023

Published: 2 March 2023



Copyright: © 2023 by the authors. Licensee MDPI, Basel, Switzerland. This article is an open access article distributed under the terms and conditions of the Creative Commons Attribution (CC BY-NC-ND) license (<https://creativecommons.org/licenses/by-nc-nd/4.0/>).

aerodynamic performance (total-to-static (t-s) pressure rise and t-s efficiency) is evaluated through steady-state CFD simulations. The meridional geometry and blade loading parameters are then parameterized using 13 parameters, and around 120 different blade geometries are generated with a wide range of variation in these 13 design parameters. T-s pressure rise and t-s efficiency values of these 120 designs are evaluated using CFD simulations. A design matrix consisting of all the design and performance parameters of these 120 designs is obtained. Kriging is used to create an RSM using the design matrix data and MOGA is used to search the optimal designs in the design space based on RSM. The final optimal design is selected from the Pareto Front and its performance is validated using CFD simulations at two operating points. The flow chart of the design and optimization process is shown in Figure 1.

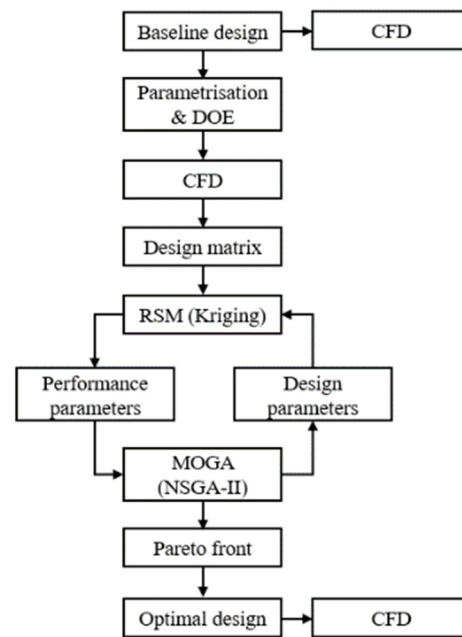


Figure 1. Flow chart of the design and optimization process.

2. Blade Design

2.1. The 3D Inverse Design Method

The 3D inverse design method, also known as the Circulation Method in the literature, is described in detail in [15]. It has been used in the design of different types of fans including axial fans [16] and centrifugal blowers [17,18]. The blade geometry is calculated iteratively based on the prescribed blade loading distribution ($\frac{\partial(r\bar{v}_\theta)}{\partial m}$, the derivative of $r\bar{v}_\theta$ along the meridional direction) on the meridional geometry; $r\bar{v}_\theta$ is the circumferentially averaged bound circulation and is defined by Equation (1) below, where r is the radius, \bar{v}_θ is the circumferential velocity and N is the blade number. For incompressible potential flow, the blade loading (the pressure difference between the pressure surface and suction surface of the blade) is defined by Equation (2), where p^+ is the static pressure on the pressure side and p^- is the static pressure on the suction side.

$$r\bar{v}_\theta = \frac{N}{2\pi} \int_0^{2\pi/N} r \cdot v_\theta d\theta \quad (1)$$

$$p^+ - p^- = \frac{2\pi}{N} \rho W_{mbl} \frac{\partial(r\bar{v}_\theta)}{\partial m} \quad (2)$$

2.2. Blade Parametrization

The main inputs for the inverse design method are meridional geometry, blade thickness distribution, blade loading and stacking. The blade meridional geometry is parametrized by eight parameters including the blade tip width (L), the hub radial length (dR_{hub}), the shroud radial length (dR_{shr}), the TE angle (α), the hub angle (β_{hub}), the shroud angle (β_{shr}), the LE curvature and the shroud curvature, as shown in the Figure 2. The blade thickness distribution is defined as 5 mm constant and the number of blades is six. LE and TE $r\bar{v}_\theta$ are used as inputs which will fix the work coefficient (specific torque/power) based on Euler’s Turbomachinery Equation. The streamwise blade loading distribution ($\frac{\partial(r\bar{v}_\theta)}{\partial m}$) is defined using a three-segment method shown in Figure 3. The loading distribution is defined by two curves at hub and shroud. For each curve, two points on the meridional location (NC and ND) divide the curve into three parts. The first and last curves are parabolic, and the middle curve is a straight line. The slope of the middle straight line is defined by a parameter called SLOPE. The loading value at LE ($m = 0$, where m is the normalized meridional coordinate) is defined by DRVT, which controls the incidence at the LE.

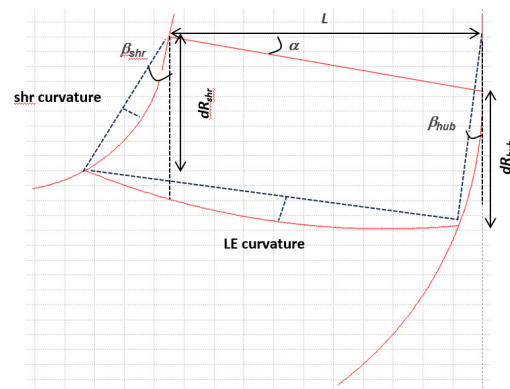


Figure 2. Meridional geometry parametrization.

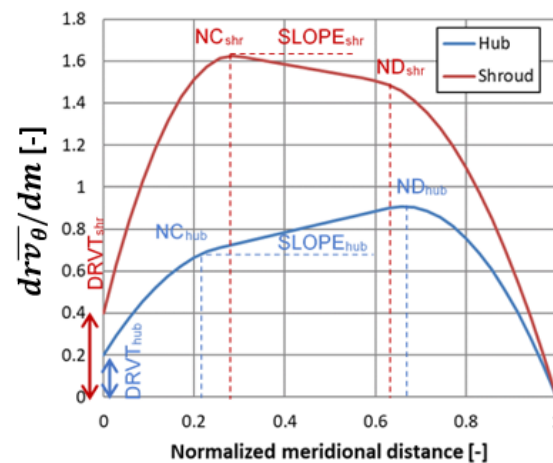


Figure 3. Streamwise blade loading defined using three-segment method.

The last input parameter required is the stacking condition, which is a spanwise wrap angle distribution at a fixed streamwise location. For fans, it is common to stack at the TE. Most of the centrifugal fans are made from sheet metal and the blade has to be 2D and axial filament. However, development in additive manufacturing can make it easier to design centrifugal fan blades with 3D geometry. The 3D inverse design method used in this study makes it quite easy to design either in 3D or in 2D. In this paper, a 2D geometry is used for the blade optimization and a zero stacking at TE is used for all the designs. Once all the

inputs are specified, the 3D inverse design method computes the blade shape for a given specified blade loading.

2.3. Design Specifications and Baseline Blade Generation

The design specifications are shown in Table 1. The fan is required to meet the minimum pressure rise requirements at two operating points (OP₁ and OP₂). The maximum torque is set by the motor provided and the main target is to maximize the efficiency at two operating points. The geometrical constraints are that the fan diameter cannot exceed the maximum value provided and the blade has to be 2D and axial filament.

Table 1. Design specifications and constraints.

Flow Coefficient	0.22
Loading Coefficient	0.39
RPM	$\leq RPM_{max}$
Volume flow rate @ OP ₁	Q_1
Pressure rise @ OP ₁	$\geq \Delta p_1$
Volume flow rate @ OP ₂	$Q_2 = 117\%Q_1$
Pressure rise @ OP ₂	$\geq \Delta p_2$
Torque	$\leq \tau_{max}$
Efficiency @ OP ₁	Maximize
Efficiency @ OP ₂	Maximize
Impeller diameter	$\geq D_{max}$
Blade	2D and axial filament

The meridional geometry of the baseline design is shown in Figure 4. The LE/TE $r\bar{v}_\theta$ and streamwise blade loading are shown in Figure 5. It is noted that LE/TE $r\bar{v}_\theta$ is normalized by the blade tip radius and tip speed. Once the solver is converged, the 3D blade from the inverse design method is converted to a 2D/axial filament blade using axial filament modification, which axially maps the wrap angle distribution of the hub to all the other spanwise layers.

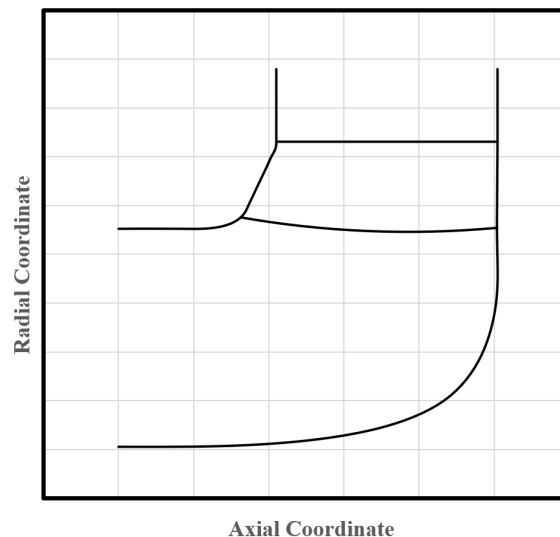


Figure 4. Baseline meridional geometry.

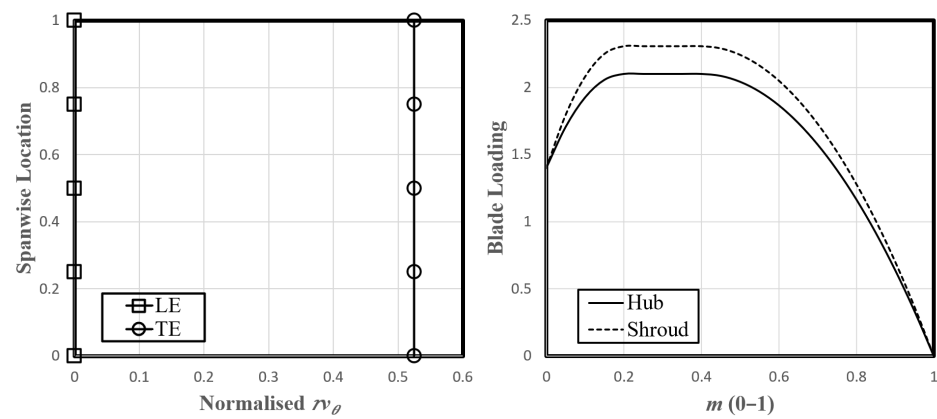


Figure 5. Baseline spanwise $r\bar{v}_\theta$ and streamwise blade loading.

3. CFD Simulation

3.1. Mesh Generation

The structured mesh was generated using ANSYS TurboGrid for the impeller blade (around 500,000 hexahedra elements) and unstructured mesh was generated for the inlet cone and inblock/outblock geometries (around 500,000 tetrahedra elements). The total number of elements is around 1,000,000. The near wall element size is 0.03 mm for the impeller and 0.05 mm for the inblock/outblock, which result in the maximum y^+ value on the walls of less than 1.0, well within the viscous sublayer; y^+ is the non-dimensional distance (based on local cell fluid velocity) from the wall to the first mesh node. The number of prism layers for the inflation is 10. As can be seen in Figure 6, the gap between the stationary inlet cone and the rotating impeller shroud casing is well resolved.

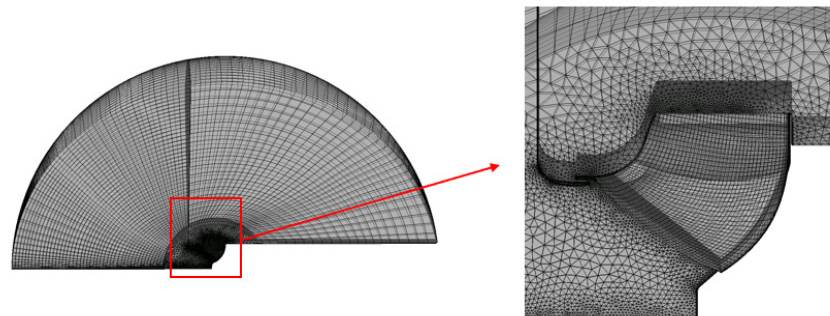


Figure 6. Computational domain.

3.2. CFD Setup

Steady-state CFD simulations (RANS) were performed by using commercial software ANSYS CFX. The inlet boundary condition is the given mass flow rate, and the outlet boundary condition is the opening with 1 atm static pressure. The impeller domain is rotational with the fixed RPM. Periodic boundary conditions were used for all domains to save the computational cost. The interface between the stationary domain and the rotational domain is set as Frozen Rotor. The turbulence model used is shear stress transport SST $k-\omega$. A high-resolution (2nd-order) advection scheme was used. The convergence criteria for the continuity and momentum equations were set as $RMS < 1.0 \times 10^{-4}$. The fan pressure rise and torque values were monitored and reach to a constant value once the solution is converged. The complete CFD model is shown in the Figure 7.

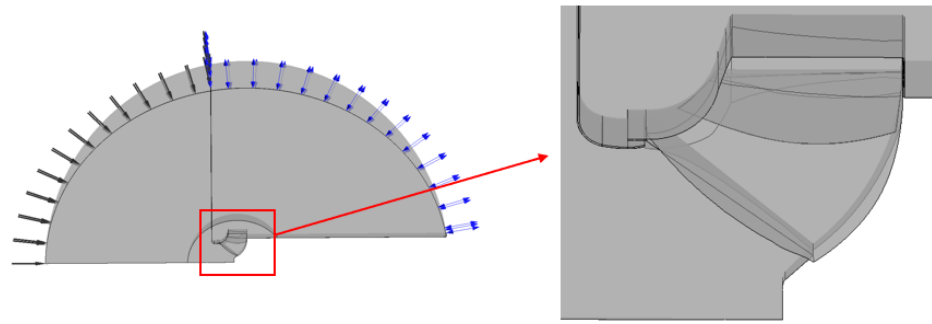


Figure 7. CFD model in ANSYS CFX.

3.3. CFD Results

Once the CFD simulations are converged, the pressure rise, torque and efficiency values can be obtained for both operating points (OP₁ and OP₂) and are summarized in Table 2. The total-to-static pressure rise is calculated as the difference between inlet total pressure and outlet static pressure. It can be seen that the baseline design almost meets the pressure rise requirements at both operating points and does not exceed the maximum torque. The efficiencies for OP₁ and OP₂ are 57.7% and 44.2%, respectively. After examining the detailed flow field, it was found that the flow behaves well at hub and mid-span locations but separates near the shroud part of the blade at OP₁ and OP₂, which can be seen in Figure 8.

Table 2. Baseline CFD results.

Variable Name	OP ₁	OP ₂
RPM	RPM_{max}	RPM_{max}
Q	Q_1	Q_2
Δp_{ts}	$0.99 \Delta p_1$	$0.94 \Delta p_2$
τ	τ_{max}	$0.91 \tau_{max}$
η_{ts}	57.7%	44.2%

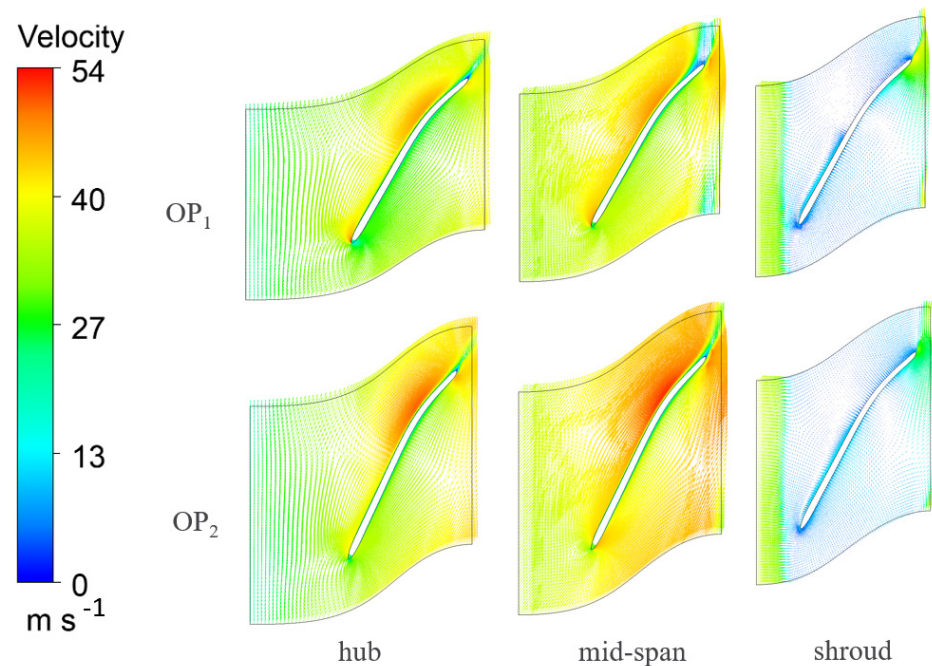


Figure 8. Baseline relative velocity vector at OP₁ and OP₂.

4. DOE and Optimization

4.1. DOE

To improve and obtain the best possible fan performance, a DOE study was performed. In total there are 13 design parameters, including 8 meridional geometry parameters and 5 loading parameters (NC, ND, SLOPE, DRVT and RVT_TE). DRVT is the streamwise loading value at LE, as shown in Figure 3, and RVT_TE is $TE \overline{r\overline{v}_\theta}$. The same values are used for hub and shroud blade loading to obtain 2D/axial filament blades. For each of the 13 design parameters, a min and max value around the baseline value is carefully specified which allows a large design space to be explored and has a good convergence rate to avoid many diverged cases in the DOE. Latin Hypercube sampling (LHS) is a statistical method which can be used to create a random sampling of multiple parameters. The number of designs has to be equal to the number of levels for each design parameter and greater than the number of the design parameters. The Optimal Latin Hypercube sampling (OLHS) is a special LHS where all the design points are equally spaced [19]. The disadvantage of OLHS is that it requires more time to generate the design matrix compared to LHS. A total of 120 different designs were generated using the OLHS method. For each design, the blade generation, meshing and CFD (two operating points) were performed automatically in ANSYS Workbench, as shown in Figure 9.

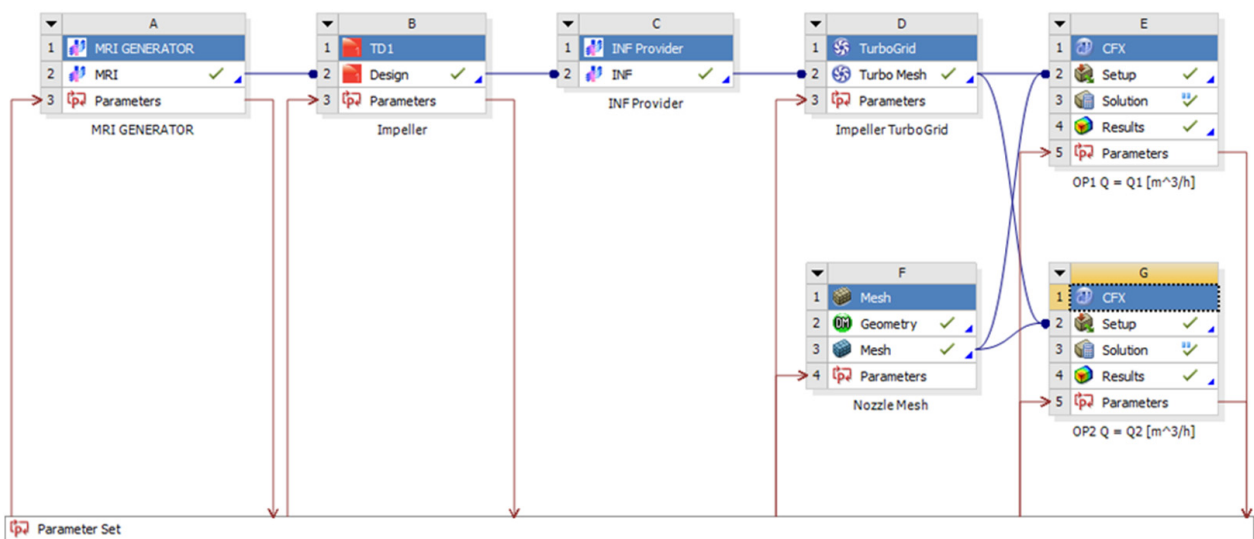


Figure 9. Automated DOE workflow in ANSYS Workbench.

Once the CFD simulations were finished, a design matrix of 120 designs with all the design parameters and performance parameters were obtained. All the CFD results are shown in Figure 10. It can be seen that a number of designs in the DOE meet the minimum pressure rise requirements at both operating points with good efficiencies compared to the baseline design. The torque values of almost all the DOE designs do not exceed the maximum constraint.

4.2. Optimization

The terms response surface model (RSM), surrogate model, approximation model and meta model are used as synonyms in the literature. The RSM is a mathematical model and constructed based on data from known designs (usually from DOE) that provides fast approximation and evaluation of objectives for different design parameters at new design points.

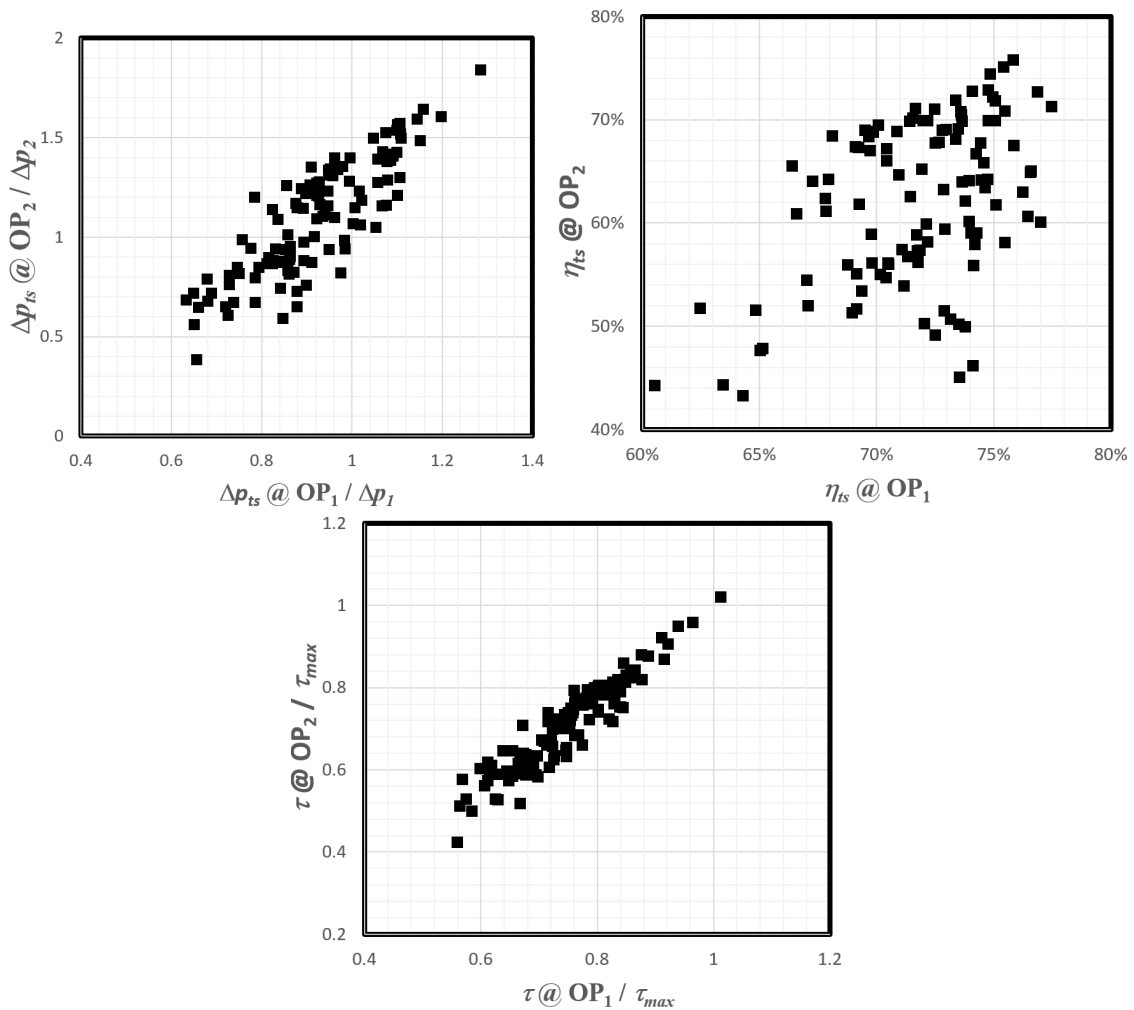


Figure 10. CFD results (pressure rise, efficiency and torque) of DOE designs.

Kriging is a method of interpolation which was first proposed by a South African statistician and mining engineer Danie G. Krige and is used to predict the location of unknown mineral resources. The basic idea of Kriging is that the value at an unknown point should be the average of the known values at its neighbors, weighted by the neighbor’s distance to the unknown point (Chung and Siller [20,21]).

MOGA (NSGA-II, non-dominated sorting genetic algorithm-II) is a multi-objective genetic algorithm which was first proposed by Deb et al. [22]. It is well-suited for highly non-linear design spaces; each objective is treated separately and a Pareto Front is constructed by selecting feasible non-dominated designs.

All the DOE results can be used to create a RSM using the Kriging approximation method. The calculated CoP (Coefficient of Prognosis) of the output parameters for the Kriging RSM is around 0.85. The optimization was performed by searching the design space with the given constraints and objectives and the performance of different designs, can be quickly evaluated through the Kriging RSM model. The constraints and objectives used in the optimization are listed in the Table 3. It is noted that ‘Angle’ is defined by Equation (3). This parameter is used to control the fan p - Q curve slope (shape) and should be kept as close as possible to the target value, which is around -5° .

$$\text{Angle} = \tan^{-1} \left(\frac{\Delta p_1 - \Delta p_2}{Q_1 - Q_2} \right) \tag{3}$$

Table 3. Optimization constraints and objectives.

$\Delta p @ OP_1$	$\geq \Delta p_1$
$\Delta p @ OP_2$	$\geq \Delta p_2$
$\tau @ OP_1$	$\geq \tau_{max}$
$\tau @ OP_2$	$\geq \tau_{max}$
Angle	$\geq -5.5^\circ$ & $\leq -4.9^\circ$
$\eta_{ts} @ OP_1$	Maximize
$\eta_{ts} @ OP_2$	Maximize

A total of 100,000 designs were generated using MOGA (NSGA-II), and the resulting Pareto Front and the selected optimal design are shown in the Figure 11. An obvious trade-off between the efficiencies at two operating points can be observed.

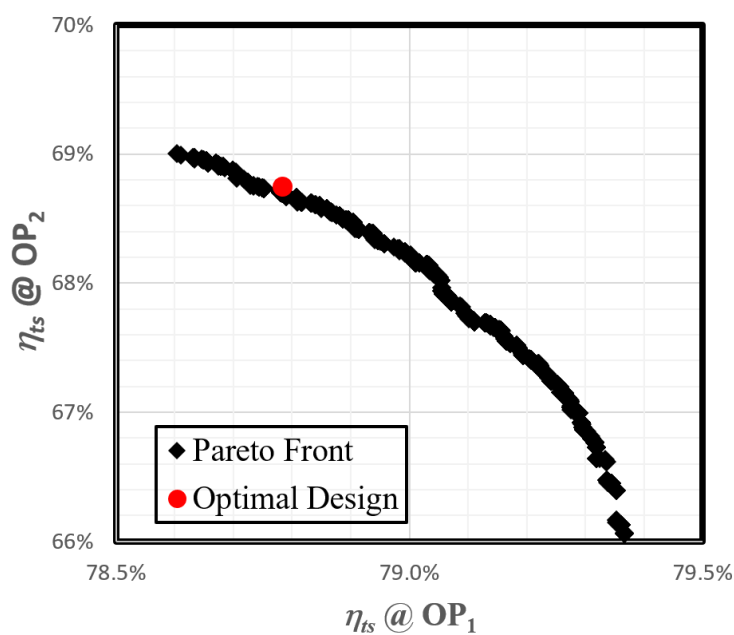


Figure 11. Pareto Front and selected optimal design.

The CFD performance of the optimal design is compared with the baseline and shown in Figure 12. The pressure rise of the optimal design is improved significantly at both operating points compared to the target and baseline values while maintaining the desirable p - Q slope (shape). The efficiencies of the optimal design are improved by around 20 percentage points at both operating points compared to the baseline design. The torque values are reduced and do not exceed the maximum constraint.

The comparison of the meridional geometry and the streamwise blade loading between the optimal design and the baseline is shown in Figure 13. The comparison of the 3D geometries of the baseline and the optimal design is shown in Figure 14.

The improvement in efficiencies can also be explained by comparing the flow fields of the two designs (Figures 7 and 15). In particular, the flow near the shroud of the optimal design is improved significantly and now fully attaches on the blade surface compared to that of the baseline design.

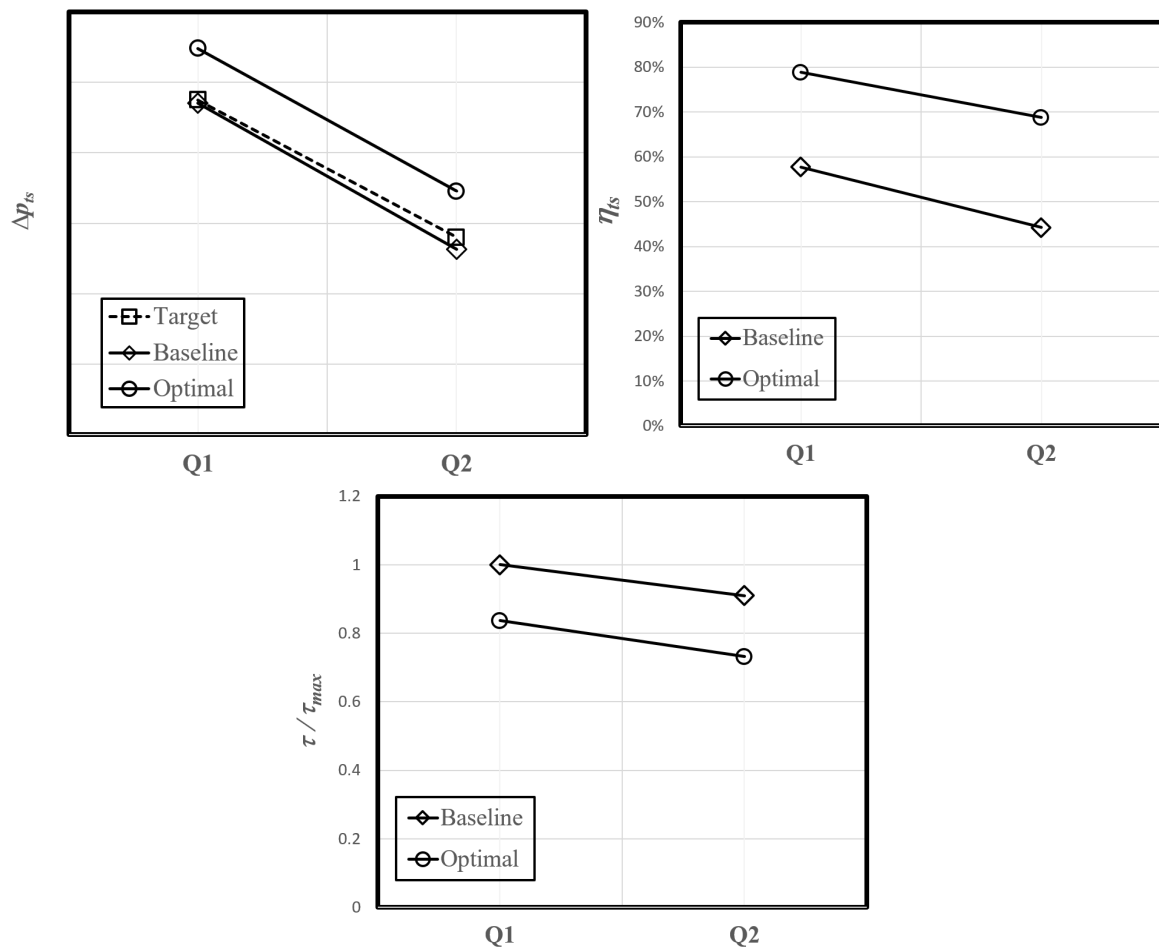


Figure 12. Comparison of CFD results for baseline and optimal design.

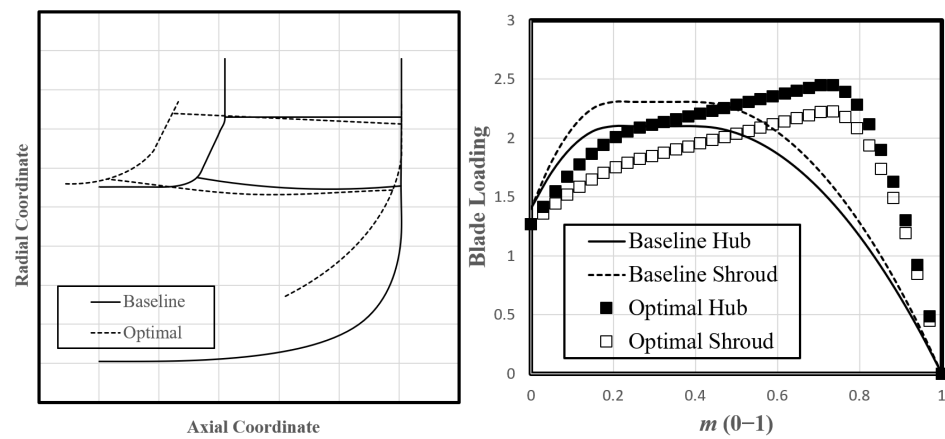


Figure 13. Comparison of meridional geometry and blade loading distribution for baseline and optimal design.

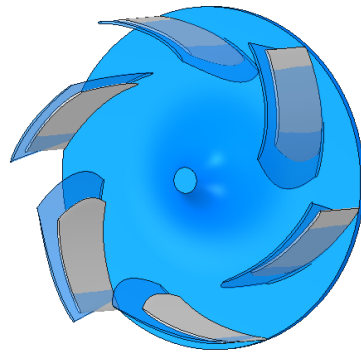


Figure 14. Comparison of 3D geometries of baseline (grey) and the optimal design (blue).

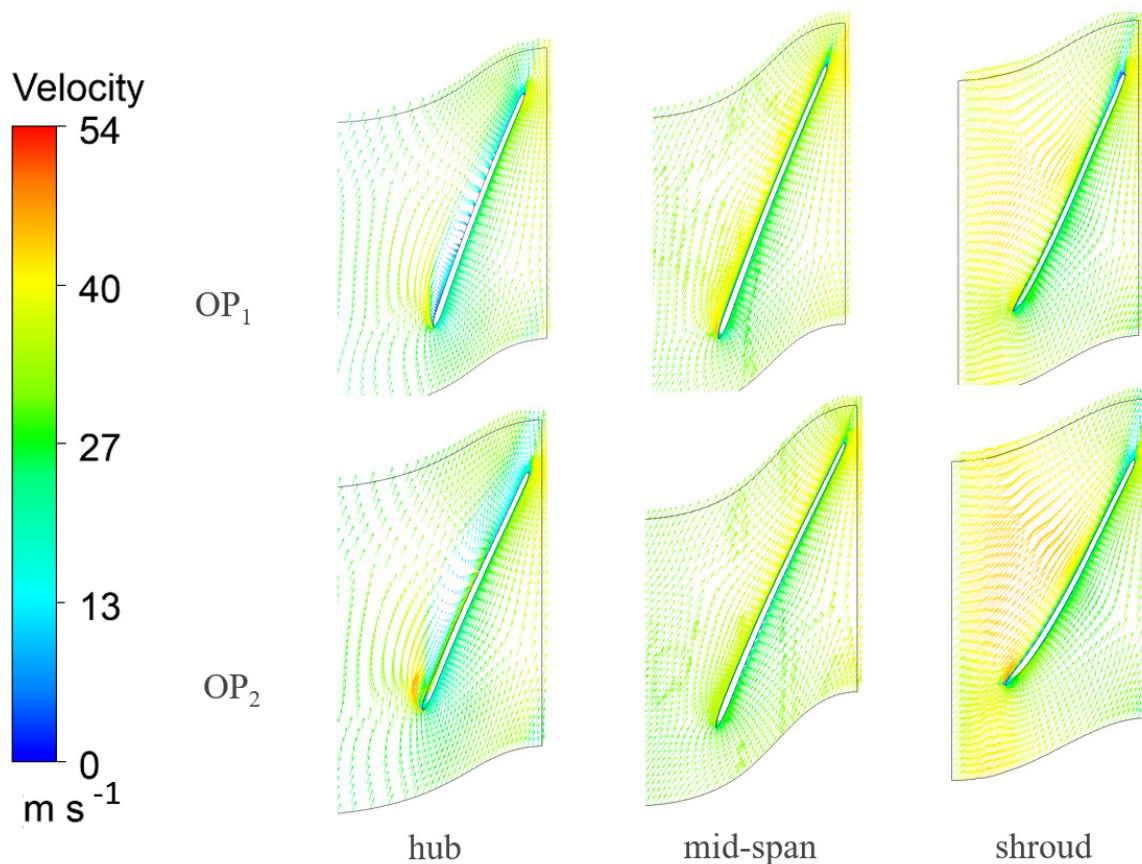


Figure 15. Optimal design relative velocity vector at OP₁ and OP₂.

5. Conclusions

In this paper, a systematic optimization methodology using the inverse design method, DOE and MOGA is presented and used to optimize the aerodynamic performance of a centrifugal fan at two operating points. The total-to-static pressure rise and total-to-static efficiencies at two operating points are improved significantly, and the improvement is validated using steady-state CFD simulations.

Author Contributions: Conceptualization, J.Z. and M.Z.; methodology, J.Z.; software, J.Z.; validation, J.Z. and M.Z.; formal analysis, J.Z.; investigation, J.Z.; resources, J.Z.; data curation, J.Z.; writing—original draft preparation, J.Z.; writing—review and editing, J.Z.; visualization, J.Z.; supervision, M.Z.; project administration, n/a; funding acquisition, n/a. All authors have read and agreed to the published version of the manuscript.

Funding: This research received no external funding.

Institutional Review Board Statement: Not applicable.

Informed Consent Statement: Not applicable.

Data Availability Statement: Not applicable.

Conflicts of Interest: The authors declare no conflict of interest.

References

1. Jeon, W.-H.; Baek, S.-J.; Kim, C.-J. Analysis of the aeroacoustic characteristics of the centrifugal fan in a vacuum cleaner. *J. Sound Vib.* **2003**, *268*, 1025–1035. [[CrossRef](#)]
2. Woodard, J.K., Jr.; Johnson, G.E. Optimal design of cooling fan for industrial electric motors. *J. Mech. Transm. Autom. Des.* **1986**, *108*, 224–266. [[CrossRef](#)]
3. Rugang, C. Experimental study on erosion characteristic for different blade contours in the centrifugal fan exposed to solid particulate environment. *Fluid Mach.* **2000**, *1*, 5–8.
4. Tan, J.; Tang, W.; Yuan, W. Optimizing technique of air-cooled engine centrifugal cooling fan test. *Chin. Intern. Combust. Engine Eng.* **2002**, 1002–6819.
5. Li, H. Flow driven by a stamped metal cooling fan—Numerical model and validation. *Exp. Therm. Fluid Sci.* **2009**, *33*, 683–694. [[CrossRef](#)]
6. Chang, C.-C.; Cheng, C.-C.; Ke, M.-T.; Chen, S.-L. Experimental and numerical investigations of air cooling for a large-scale motor. *Int. J. Rotating Mach.* **2009**, *2009*, 34–40. [[CrossRef](#)]
7. Hariharan, C.; Govardhan, M. Effect of inlet clearance on the aerodynamic performance of a centrifugal blower. *Int. J. Turbo Jet Engines* **2016**, *33*, 215–228. [[CrossRef](#)]
8. Singh, O.P.; Khilwani, R.; Sreenivasulu, T.; Kannan, M. Parametric Study of Centrifugal Fan Performance: Experiments and Numerical Simulation. *Int. J. Adv. Eng. Technol.* **2011**, *1*, 33–50.
9. Jeon, W.-H. A numerical study on the effects of design parameters on the performance and noise of a centrifugal fan. *J. Sound Vib.* **2003**, *265*, 221–230. [[CrossRef](#)]
10. Pei, J.; Wang, W.; Yuan, S.; Zhang, J. Optimization on the Impeller of a Low-specific-speed centrifugal Pump for hydraulic Performance Improvement. *Chin. J. Mech. Eng.* **2016**, *29*, 992–1002. [[CrossRef](#)]
11. Zhang, J.; Zangeneh, M. Multidisciplinary and multi-point optimisation of radial and mixed-inflow turbines for turbochargers using 3D inverse design method. In *The 14th International Conference on Turbochargers and Turbocharging*; CRC Press: London, UK, 2020.
12. Tuchler, S.; Chen, Z.; Copeland, C.D. Multipoint shape optimisation of an automotive radial compressor using a coupled computational fluid dynamics and genetic algorithm approach. *Energy* **2018**, *165*, 543–561. [[CrossRef](#)]
13. Behzadmehr, A.; Piaud, J.B. Aero-Acoustical Effects of Some Parameters of a Backward-Curved Centrifugal Fan Using DOE. *HVAC&R Res.* **2006**, *12*, 353–365.
14. Qiu, S.; Deng, X. Multi-point design Optimization of a High Bypass Ratio Fan Blade. In Proceedings of the 30th Congress of the International Council of the Aeronautical Sciences, Daejeon, Republic of Korea, 25–30 September 2016.
15. Zangeneh, M. A compressible three-dimensional design method for radial and mixed flow turbomachinery blades. *Int. J. Numer. Methods Fluids* **1991**, *13*, 599–624. [[CrossRef](#)]
16. Okamoto, H.; Zangeneh, M.; Watanabe, H.; Goto, A. Design of a box fan rotor using 3-D inverse design method. In Proceedings of the IMechE International Conference on Fans, London, UK, 9–10 November 2004.
17. Henner, M.; Neddadi, Y.; Demory, B.; Zangeneh, M.; Pengie, F. Automotive blower design with inverse method applied on wheel and volute. In Proceedings of the Fan 2015, International Conference on Fan Noise, Technology and Numerical Methods, Lyon, France, 15–17 April 2015.
18. Eisenmenger, C.; Frank, S.; Dogan, H.; Ochmann, M. Aerodynamic and aeroacoustic optimization of a small centrifugal fan with backward-curved blades by means of inverse design. In Proceedings of the 23rd International Congress on Acoustics, Aachen, Germany, 9–13 September 2019.
19. Park, J.-S. Optimal Latin-hypercube designs for computer experiments. *J. Stat. Plan. Inference* **1994**, *39*, 95–111. [[CrossRef](#)]
20. Chung, H.-S.; Alonso, J.J. Multiobjective Optimization using Approximation Model-based Genetic Algorithm. In Proceedings of the 10th AIAA/ISSMO Symposium on Multidisciplinary Analysis and Optimization, Albany, NY, USA, 30 August–1 September 2004.
21. Siller, K.; Vob, S.; Nicke, E. Automated Multidisciplinary Optimization of A Transonic Axial Compressor. In Proceedings of the 47th AIAA Aerospace Science Meeting including the New Horizons Forum and Aerospace Exposition, Orlando, FL, USA, 5–8 January 2009.
22. Deb, K.; Agrawal, S.; Pratap, A.; Meyarivan, T. A Fast Elitist Non-dominated Sorting Genetic Algorithm for Multi-objective Optimization: NSGA-II. In Proceedings of the Parallel Problem Solving from Nature VI Conference, Paris, France, 18–20 September 2000; pp. 849–858.

Disclaimer/Publisher’s Note: The statements, opinions and data contained in all publications are solely those of the individual author(s) and contributor(s) and not of MDPI and/or the editor(s). MDPI and/or the editor(s) disclaim responsibility for any injury to people or property resulting from any ideas, methods, instructions or products referred to in the content.